Israel Journal of Chemistry *Vol. 49* *2009* *pp. 199–216*
DOI: 10.1560/IJC.49.2.199

OHO Hydrogen Bond Geometries and NMR Chemical Shifts: From Equilibrium Structures to Geometric H/D Isotope Effects, with Applications for Water, Protonated Water, and Compressed Ice

Hans-Heinrich Limbach,[a,*] Peter M. Tolstoy,[a] Natalia Pérez-Hernández,[a,†] Jing Guo,[a] Ilya G. Shenderovich,[a] and Gleb S. Denisov[b]

[a]Institut für Chemie und Biochemie, Freie Universität Berlin, Takustrasse 3, D-14195 Berlin, Germany
[b]Institute of Physics, St. Petersburg State University, 198504 St. Petersburg, Russia

(Received 24 November 2008 and in revised form 13 February 2009)

Abstract. Hydrogen bond geometries and ^{1}H NMR chemical shifts of OHO hydrogen-bonded systems have been analyzed using an improved valence bond order model. This model predicts that the heavy atom hydrogen bond coordinate $q_2 = r_1 + r_2$ is a function of the proton coordinate $q_1 = ½(r_1 - r_2)$, where r_1 and r_2 represent the OH and the HO distances.

In the first part, it is shown that this correlation reproduces published equilibrium geometries of the Zundel cation $H_5O_2^+$ as well as those of water clusters in the gas phase and embedded in the fullerene C180. Using the example of the water hexamer, it is shown that changing the level of calculation shifts the calculated geometries along the correlation curve, but not away from the curve. In order to take quantum zero-point vibrational effects (QZPVE) into account, an empirical correction is proposed. It is shown that this correction properly describes the calculated classical and quantum hydrogen bond geometries of compressed ice as well as calculated geometric H/D isotope effects. The improved valence bond order model is used to analyze a large number of OHO hydrogen bond geometries contained in the Cambridge Structural Database.

In the second part, a relation between the geometries and the ^{1}H NMR chemical shieldings of OHO hydrogen bonded systems is established using the valence bond order model. GIAO calculations of the isolated symmetric Zundel cation where H is located in the hydrogen bond center show only a small dependence of the chemical shifts on the O...O distance. This result is rationalized in terms of neighbor group effects and deshielding in the naked proton. The consequence is that the ^{1}H NMR chemical shifts are not much affected by QZPVE. Calculations on water clusters indicate that the influence of the chemical environment of the OHO hydrogen bonds on their ^{1}H NMR chemical shifts is smaller for the strong hydrogen bond regime but large for the weak hydrogen bond regime. A simple chemical shift vs. q_1 relation is then used to calculate the average chemical shifts of water clusters in the regime of fast hydrogen bond exchange between hydrogen bonded and free OH groups. It is shown that average chemical shifts of about 6 ppm are possible as the clusters considered exhibit a broad distribution of stronger and weaker hydrogen bonds. The implications for water in organic solvents and for liquid water are discussed, based on published data on the ^{1}H chemical shift distribution in the latter.

This paper was presented at the Research Workshop of the Israel Science Foundation: Diffusion, Solvation and Transport of Protons in Complex and Biological Systems, Elat, Israel, 13–17 January 2008.

*Author to whom correspondence should be addressed.
E-mail: limbach@chemie.fu-berlin.de
†Present address: Instituto de Investigaciones Químicas, CSIC, Avda. Américo Vespucio 49, 41092 Seville, Spain.

INTRODUCTION

Hydrogen bonding and transfer are important phenomena in nature. The geometries of hydrogen bridges have conveniently been studied in crystalline solids using X-ray diffraction, neutron diffraction,[1] and by dipolar solid state NMR techniques.[2–6] Scheme 1a depicts the "shapes",[7] i.e., thermal ellipsoids, of the three atoms of a typical hydrogen bond. Because of the large zero-point energy of H it exhibits a certain delocalization, generally described by an ellipsoid. The latter is oriented in a certain way with respect to the heavy atom axis.[7] When hydrogen bond geometries are discussed, often only the average nuclear positions are considered, as illustrated by Scheme 1b. They can be defined in terms of the two hydrogen bond distances r_1 and r_2 and the hydrogen bond angle α.

A major advancement has been the finding of correlations between the two hydrogen bond distances r_1 and r_2 (Scheme 1) based on neutron structures of OHO-systems,[8] NHN-systems,[9] NHO-systems, and other systems[10,11] assembled in the Cambridge Structural Database (CSD). Both the hydrogen bond angle α as well as the shape of the proton do not seem to play an important role in these correlations. They can be described in terms of valence bond orders proposed by Pauling[12] and Brown.[13] This concept has been used by Dunitz and coworkers[14] in order to map pathways of chemical reactions using series of crystallographic structures. It has been applied by Truhlar[15] and Agmon[16] in order to simplify the theoretical description of gas phase reactions. Recently, Agmon and coworkers used this concept for the description of proton transfer events in water.[17] For halogen- and nitrogen-containing hydrogen bonds it has been shown[4,18–21] that these correlations also come out of ab initio calculations of equilibrium structures. In order to be able to describe H/D isotope effects on hydrogen bond geometries, some of us have proposed an empirical correction that takes into account quantum zero-point vibrational effects (QZPVE). This method has been applied previously for NHN[22] and OHN hydrogen bonds,[23] and in particular to describe H/D isotope effects on their NMR parameters. The first goal of this paper is, therefore, to extend this treatment also to OHO hydrogen bonds. For that purpose, we have performed a new CSD and NMR search for geometric OHO–hydrogen bond correlations including ^{1}H chemical shifts. Moreover, we have also calculated the equilibrium geometries of OHO hydrogen bonds of water clusters in the gas phase and confined in fullerenes, as well as of protonated water molecules. We show that these data provide the best basis to set up geometric H-bond correlations. The experimental correlations allow one then to define the QZPVE contributions. In this way, we have improved the geometry–chemical shift correlations established previously by solid state ^{1}H MAS NMR and neutron diffraction. A second goal of this work is to test our empirical QZPVE method using two examples of OHO bonds where a full quantum-mechanical treatment is available. The first refers to a recent study of Kiefer and Hynes[29] of the geometric changes including H/D isotope effects during a thermally activated hydron transfer in strong OHO hydrogen bonds. This work uses a valence bond model for a strong OHO H-bond potential similar to what was used previously.[30] We show that the QZPVE method is able to describe this situation. A second example is the behavior of the hydrogen bond geometries of water in ice under high pressure, leading to a symmetrization of the OHO hydrogen bonds, which was theoretically described by Benoit, Marx and Parrinello.[7,31] The geometric response has been shown to be different for a quantum proton as compared to a classical proton. Finally, we discuss a recent study of Sebastiani and coworkers,[32] who calculated the ^{1}H chemical shift distribution function of pure water and HCl containing water. Our correlations imply that the symmetrical Zundel cation is absent in these solutions.

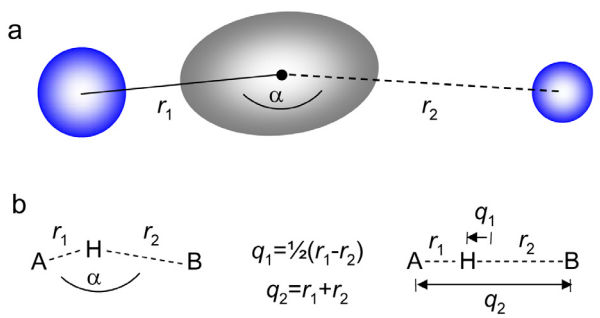

Scheme 1. Definition of hydrogen bond coordinates q_1 and q_2.

This paper is organized as follows. In the Theoretical Section the empirical correction method is described. At the same time, a numerical instability observed previously[21,22] is removed. Then, the results of the DFT calculations are reported, corrected for QZPVE, and finally compared to distance information derived from hydrogen bond correlations.

THEORETICAL SECTION

In this section we discuss geometric and NMR parameter correlations for OHO hydrogen bonds. These correlations will provide a frame for the discussion of the results presented below.

OHO–Hydrogen Bond Correlations

One can associate to any hydrogen-bonded system A–H···B, two distances $r_1 = r_{AH}$ and $r_2 = r_{HB}$ and a hy-

drogen bond angle α, as indicated in Scheme 1. It is convenient to define additionally the natural hydrogen bond coordinates q_1 and q_2 according to

$$q_1 = ½ (r_1 - r_2),\ q_2 = r_1 + r_2 \quad (1)$$

In the case of a linear hydrogen bond, q_1 corresponds directly to the distance of the proton with respect to the hydrogen bond center and q_2 to the heavy atom A···B distance.

According to the valence bond order concept,[12,13] one can associate to both hydrogen bond distances valence bond orders given by

$$p_1 = \exp\{-(r_1 - r_1^o)/b_1\} \text{ and } p_2 = \exp\{-(r_2 - r_2^o)/b_2\} \quad (2)$$

r_1^o and r_2^o represent the equilibrium distances in the fictive free diatomic units AH and HB, and b_1 and b_2 describe bond order decays with increasing bond distances.

Within this concept there is no principal difference between the "covalent" A–H and the "hydrogen bond" H...B besides different valence bond orders and bond distances. As the total valency of hydrogen is unity it follows that

$$p_1 + p_2 = \exp\{-(r_1 - r_1^o)/b_1\} + \exp\{-(r_2 - r_2^o)/b_2\} = 1 \quad (3)$$

Thus, both distances r_1 and r_2 depend on each other. Using eq 3, it is possible to express r_1 as a function of r_2, or q_1 as a function of q_2. For the case where both heavy atoms of the hydrogen bond are the same, i.e., when $b_1 = b_2 = b$ and $r_1^o = r_2^o = r^o$, it follows that[4]

$$q_2 = r_1 + r_2 = 2\ r^o + 2\ q_1 + 2b \ln[1 + \exp\{-2q_1/b\}] \quad (4)$$

The parameter b can be expressed as

$$b = [q_{2min} - 2r^o]/2\ln 2 \quad (5)$$

Here, $q_{2min} = (r_1 + r_2)_{min}$ represents a minimum value corresponding to the minimum distance A...B in the case of a linear hydrogen bond. At this point the valence bond order of each bond is ½. Thus, in eq 4 it is possible to use either b or q_{2min} as parameter.

Gilli et al.[11] and Steiner and Saenger[8–10] showed the validity of eq 4 on the basis of a number of neutron diffraction structures contained in the CSD. A more detailed analysis of NHN– and OHN–hydrogen-bonded systems showed recently that the parameters in eq 4 depend on whether strong hydrogen bonds are included or not.[22,23] In other words, it is not possible to describe both strong and weak hydrogen bonds in terms of eq 4 alone. By contrast, eq 4 could describe the results of ab initio calculations of equilibrium structures. Therefore, it was assumed that eq 4 is valid only in the absence of quantum zero-point vibrational effects (QZPVE) present in strong hydrogen bonds, which are especially strong because of large anharmonicities.[22] Both phenomena depend on the isotope L = H, D.

We proposed, therefore, to calculate the true bond orders p_{AL} and p_{LB} of ALB hydrogen bonds as a function of the equilibrium bond orders accessible by ab initio calculations in the following way[21,22]

$$p_{AL} = \exp\{-(r_{AL} - r_1^o)/b_1\} = p_1 - c^L(p_1p_2)^f(p_1 - p_2) - d^L(p_1p_2)^g$$

$$p_{LB} = \exp\{-(r_{LB} - r_2^o)/b_2\} = p_2 + c^L(p_1p_2)^f(p_1 - p_2) - d^L(p_1p_2)^g \quad (6)$$

The parameters c^L and d^L determine the size of the isotope-sensitive correction term for QZPVE. c^L describes isotope shifts along the correlation line, keeping the total bond valencies of H and of D equal to unity (eq 3). By contrast, d^L describes the deviation of the total valency of the hydrons from unity; this term leads to a flattening of the correlation curve q_1 vs. q_2 in the minimum. f and g are empirical numbers and may depend on the system studied.

Equation 6 allows one to calculate the so-called *primary geometric hydrogen bond isotope effect* (primary GIE),[4]

$$\Delta q_1 = q_{1D} - q_{1H} \quad (7)$$

and the *secondary geometric hydrogen bond isotope effect* (secondary GIE),

$$\Delta q_2 = q_{2D} - q_{2H} \quad (8)$$

The secondary effect has also been called the "Ubbelohde effect", as it was observed by Ubbelohde for a number of hydrogen-bonded systems.[33] It describes a different heavy atom position after isotopic substitution. By contrast, the *primary geometric isotope effect* describes a different location of hydrogen isotopes in the hydrogen bond.

Equation 6 worked well in the region of strong hydrogen bonds,[22,23] but we noticed a numerical instability in the region of weak hydrogen bonds. In order to remove this instability, we introduce here the following changes of eq 6:

$$p_{AL} = \exp\{-(r_{AL} - r_1^o)/b_1\} = p_{1L}^* - 2d^L p_1(p_{1L}^* p_{2L}^*)^g,$$

$$p_{LB} = \exp\{-(r_{LB} - r_2^o)/b_2\} = p_{2L}^* - 2d^L p_2(p_{1L}^* p_{2L}^*)^g,$$

$$p_{1L}^* = p_1 - c^L(p_1p_2)^f(p_1 - p_2),$$

$$p_{2L}^* = p_2 + c^L(p_1p_2)^f(p_1 - p_2) \quad (9)$$

These changes, which are purely empirical, removed the numerical instabilities in a satisfactory way.

This hydrogen bond correlation procedure does not hold under large pressures. The latter may lead to a situation where the minimum distance may be further reduced by placing the molecular system of interest in a confining volume. We assume the following relation

$$b = (q_{2\min} - 4t(p_1p_2) - 2r_o)/2\ln 2 \quad (10)$$

Here, t represents a parameter describing the reduction of the minimum distance induced by the confinement.

The NMR parameters of hydrogen bonds can be related to their geometries. For example, Benedict et al. have proposed to express ^{1}H chemical shifts as a function of the valence bond orders[34]

$$\delta_{A\underline{H}B} \equiv \delta_H = \delta_{A\underline{H}}{}^o p_1 + \delta_{\underline{H}B}{}^o p_2 + \Delta_{A\underline{H}B}(4p_1p_2)^m \quad (11)$$

$\delta_{A\underline{H}}{}^o$ and $\delta_{\underline{H}B}{}^o$ are the limiting chemical shifts of the separate fictive groups AH and BH. The last term represents an excess hydrogen bond shift that is equal to $\Delta_{A\underline{H}B} \equiv \Delta_H$ for a symmetric or quasisymmetric complex with $p_1 = p_2 = 0.5$. m is an empirical fitting parameter with a value normally set to unity. As eq 11 is only valid for equilibrium structures, we take QZPVE into account by assuming that

$$\delta_{A\underline{H}B} \equiv \delta_H = \delta_{A\underline{H}}{}^o p_1 + \delta_{\underline{H}B}{}^o p_2 + \Delta_{A\underline{H}B}{}^*(4\, p_{AH}{}^* \, p_{HB}{}^*)^m \quad (12)$$

The last term may be different from the corresponding term in eq 11. As $p_{AH}{}^*$ and $p_{HB}{}^*$ are smaller than 0.5 for a symmetric or a quasisymmetric complex, $\Delta_{A\underline{H}B}{}^*$ may be larger than $\Delta_{A\underline{H}B}$.

Ab Initio and Chemical Shift Calculations

The structures of various systems containing free OH groups or OHO hydrogen bonds were calculated using the Gaussian 03 set of programs[35] at the MP2/6-311++G** level of theory.[36] Generally the structures obtained correspond to the optimized geometries of the equilibrium structures of the isolated systems. The same program system also allowed us to calculate the GIAO nuclear magnetic shielding values of all nuclei, but only the ^{1}H values were analyzed.

RESULTS AND DISCUSSION

In this section we will discuss correlations between the geometries and ^{1}H NMR chemical shifts of OHO hydrogen bonds in various systems and environments. The correlation curves presented were calculated using the equations described in the previous section, and the parameters listed in Table 1.

Table 1. Parameters of the correlation lines in Figs. 1 to 7

	eq	r^o/Å	$q_{2\min}$/Å	b/Å	f	g	c^H	d^H	c^D	d^D	t/Å	$\delta_{OH}{}^o$ /ppm	Δ_H or $\Delta_H{}^*$ /ppm	m
Fig. 1 solid line	(4),(5)	0.96	2.38	0.332	–	–	–	–	–	–	–	–	–	
Fig. 1 dotted line	(4),(5),(6)	0.96	2.38	0.332	5	2	360	0.6	0	0	0	–	–	
Fig. 2 solid line	(4),(5)	0.93	2.36	0.36	–	–	–	–	–	–	–	–	–	
Fig. 2 dotted line	(4),(5),(6)	0.93	2.36	0.36	5	2	360	0.6	0	0	0	–	–	
Fig. 3 dashed curve 3	(4),(5)	0.93	2.36	0.36	–	–	–	–	–	–	–	–	–	
Fig. 3 solid line 100 K curve 1	(10)	0.93	2.36	0.36	–	–	–	–	–	–	0.1	–	–	
Fig. 3 dotted line 100 K curve 2	(4),(5),(9), (10)	0.93	2.36	0.36	5	2	0	0.85	–	–	–	–	–	
Fig. 4a solid line	(4),(5),(9)	0.96	2.38	0.332	–	–	–	–	–	–	–	–	–	
Fig. 4a dotted line	(4),(5),(6), (9)	0.96	2.38	0.332	4	2	43	2.1	–	–	–	–	–	
Fig. 4b dotted line	(4),(5),(6), (9)	0.96	2.38	0.332	4	2	43	2.1	8	2.08	0	–	–	
Fig. 4c dotted line	(4),(5),(9), (10)	0.96	2.38	0.332	4	2	43	2.1	8	2.08	0	–	–	
Fig. 5a solid line 1	(4),(5),(11)	0.93	2.36	0.36	–	–	–	–	–	–	–	0.73	20	1.1
Fig. 5a solid line 2	(4),(5),(11)	0.93	2.36	0.36	–	–	–	–	–	–	–	7.9	13	1.1
Fig. 5a dotted line 3	(4),(5),(12)	0.93	2.36	0.36	5	2	360	0.6	–	–	–	7.9	16	1.4
Fig. 5b solid line	(4),(5),(11)	0.93	2.36	0.36	–	–	–	–	–	–	–	0.73	20	1.1
Fig. 7 dotted line 1	(4),(5),(12)	0.93	2.36	0.36	5	2	360	0.6	–	–	–	0.73	23.8	1.2
Fig. 7 dotted line 2	(4),(5),(12)	0.93	2.36	0.36	5	2	360	0.6	–	–	–	6.0	17.5	1.2
Fig. 7 dashed line 3	$\delta_H = 0.73 + 19.8 \exp(-6.2\, q_1{}^2)$													
Fig. 7 dashed line 4	$\delta_H = 6 + 14.5 \exp(-6.2\, q_1{}^2)$													

Classical OHO Correlation from Computed Equilibrium Geometries

Figure 1 depicts a graph of the heavy atom coordinate $q_2 = r_1 + r_2 = r_{OH} + r_{HO}$ of OHO hydrogen bonds as a function of the proton coordinate $q_1 = ½(r_1 - r_2) = ½(r_{OH} - r_{HO})$. When H is shifted from the left oxygen to the right one, the O...O distance decreases, goes through a minimum at $q_1 = 0$, and increases again. The data points were calculated for the equilibrium structures of various water species by different authors using various ab initio methods. Included are the data of the isolated water dimer and trimer calculated by Gerber and coworkers.[37] The data point at $q_1 = 0$, calculated by Sobolewski and Domcke[38] and confirmed by Del Bene et al.,[39] refers to the isolated protonated water dimer or the "Zundel cation", exhibiting a single well potential for the proton motion. In this symmetric hydrogen bridge, H is shared by both oxygen atoms. All these data points are assembled in Table 2. Not contained are the data points characterized by the crosses in Fig. 1. They refer to the geometries of water clusters $(H_2O)_n$, $n = 2$ to 16 confined in fullerene C180 calculated by Wang et al.[40] These data points are available in the supplementary information of ref 40 as well as in Table S1 of the Supporting Information (DOI: 10.1560/IJC.49.2.S1). The confinement of large clusters in the fullerene leads to hydrogen bond compression and hence to a decrease of the O...O distances as compared to free water clusters. It is strongest in one of the hydrogen bonds of a cluster cage $(H_2O)_{16}$, which exhibits ten faces, constructed by two cyclic tetramers and eight cyclic pentamers.

In this study we wanted to check how the level of theory used in the calculations affects the results.

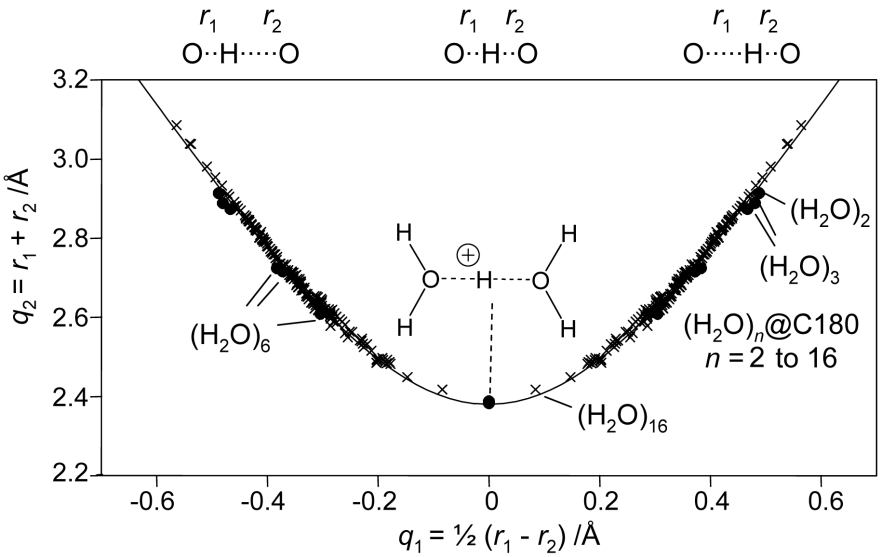

Fig. 1. Hydrogen bond correlation q_2 vs. q_1 of the calculated equilibrium geometries of water dimers,[37] the protonated water dimer,[38,39] and of water clusters $(H_2O)_n$, $n = 2$ to 16 confined in fullerene C180.[40] The correlation curve was calculated using the parameters listed in Table 1.

Table 2. Calculated hydrogen bond geometries of water clusters and the protonated water dimer

system	method	reference	q_1/Å	q_2/Å	r_1/Å	r_2/Å
$H_5O_2^+/C_2$	MP2/6-311++G**	this work	0	2.383	1.1916	1.1916
$H_5O_2^+/C_2$	MP2/6-31+G**	38	0	2.388	1.194	1.194
$H_5O_2^+/C_2$	B3LYP/6-31+G**	38	0	2.402	1.201	1.201
$H_5O_2^+/C_2$	MP2/6-31+G(d,p)	39	0	2.386	1.193	1.193
$(H_2O)_2$	MP2/6-31+G(d,p)	39	0.488	2.916	1.946	0.970
$(H_2O)_2$	MP2/TZP	37	0.4805	2.889	1.925	0.964
cyclic $(H_2O)_3$	MP2/TZP	37	0,467	2,874	0.97a	1,904
cyclic $(H_2O)_3$	MP2/TZP	37	0,4525	2,845	0.97a	1,875
cyclic $(H_2O)_6$	B3LYP/6-311++G**	this work	0.3723	2.7162	1.7304	0.9858
cyclic $(H_2O)_6$	MP2/6-311G	this work	0.3044	2.6090	1.6089	1.0001
cyclic $(H_2O)_6$	MP2/6-311++G**	this work	0.3829	2.7243	1.7450	0.9793
cyclic $(H_2O)_6$	HF/6-311G	this work	0.3583	2.6507	1.6837	0.9670

TZP: triple-ζ basis set with polarization.

Therefore, we have calculated the cyclic water hexamer $(H_2O)_6$ using different methods and basis sets. The results are included in Table 2 and in Fig. 1.

The solid line was calculated using eq 4. The parameters $r^o = 0.96$ Å and $b = 0.33$ Å were obtained by fitting the data to eq 4. This fit is very satisfactory. We note that r^o is close to the O...H distance of 0.963 Å of isolated H_2O.[39] From the value of b we calculate a minimum O...O distance of 2.38 Å, which is close to the O...O distance in the Zundel cation.[38,39] Small deviations arise from the simplification made in eq 4. As only calculated equilibrium structures are considered in Fig. 1, no QZ-PVE correction was applied.

We note that changing the calculation method can lead to large changes of the hydrogen bond geometries. However, we note that the calculated geometries are shifted along the correlation curve, but not away from the curve. Thus, almost all calculated geometries in Fig. 1 are located on the correlation curve, independently of the method of calculation used.

OHO Correlations from Experimental Neutron Structures

In Fig. 2 we have plotted experimental data points q_2 vs. q_1 obtained from the neutron structures contained in the Cambridge Structural Database of crystalline solids

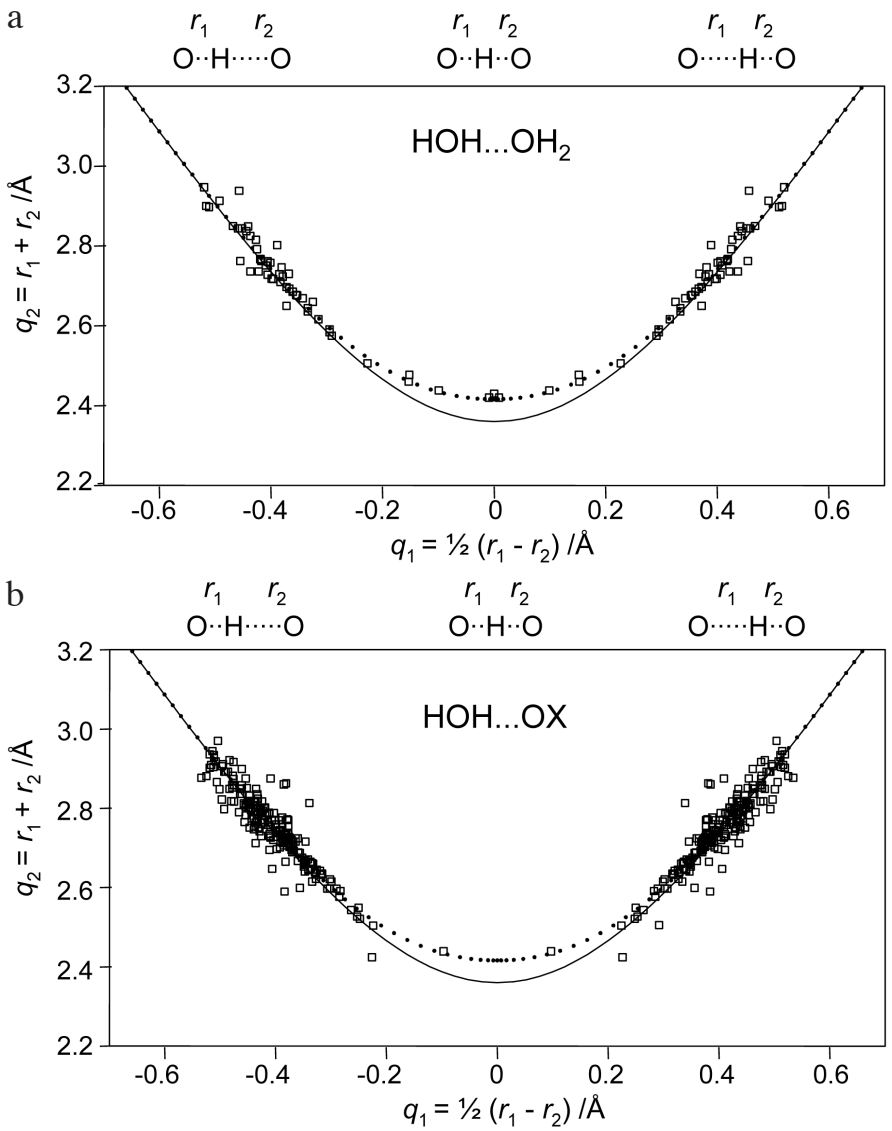

Fig. 2. Hydrogen bond correlation q_2 vs. q_1 of the neutron structures contained in the Cambridge Structural Database of systems exhibiting OHO hydrogen bonds in the solid state. The solid lines refer to correlation equilibrium geometries (eq 4). The dotted lines were calculated using the empirical quantum correction of eq 9. (a) OHO hydrogen bonds between water molecules in water-containing solids. (b) OHO hydrogen bonds between water molecules and oxygen atoms in water-containing solids.

containing OHO hydrogen bonds. Figures 2a and 2b contain bonds between water molecules, and of water to oxygen in organic molecules. Figure 2c contains data from XOHOY bonds, where X, Y = carbon, and Fig. 2d from bonds with X, Y, or both are atoms other than carbon. In the case of Figs. 2a, 2b, and 2d, the scattering of the data is less pronounced in the case of the strong hydrogen bonds around $q_1 = 0$, in contrast to the weaker hydrogen bonds. However, a large scattering is also found for the strong COHOC hydrogen bonds (Fig. 2c). In this region, around $q_1 = 0$, substantially larger values of q_2 are observed as compared to $q_{2\min}$. In most cases this arises from a proton tautomerism between two different forms, where the proton transfer experiences a barrier through which it can tunnel or over which it can jump.[41]

The solid lines in Fig. 2 were calculated without the QZPVE correction (eq 4), and the dotted lines with the QZPVE correction (eq 9). The main difference is that in the strong hydrogen bond range around $q_1 = 0$ the heavy atom coordinate q_2, which is close to the O...O distance, is larger than the minimum value corresponding to the equilibrium structure because of the width of the zero-point vibration of H. This effect is smaller for D, as will be discussed in the next section.

In Fig. 2a some data points appear at $q_1 = 0$ and $q_2 \approx 2.4$ Å that correspond to water clusters in solids containing an excess proton, exhibiting motifs such as the Zundel cation. It is astonishing that the O...O distances in these condensed matter Zundel cations are almost the same as in the isolated ion. The data points

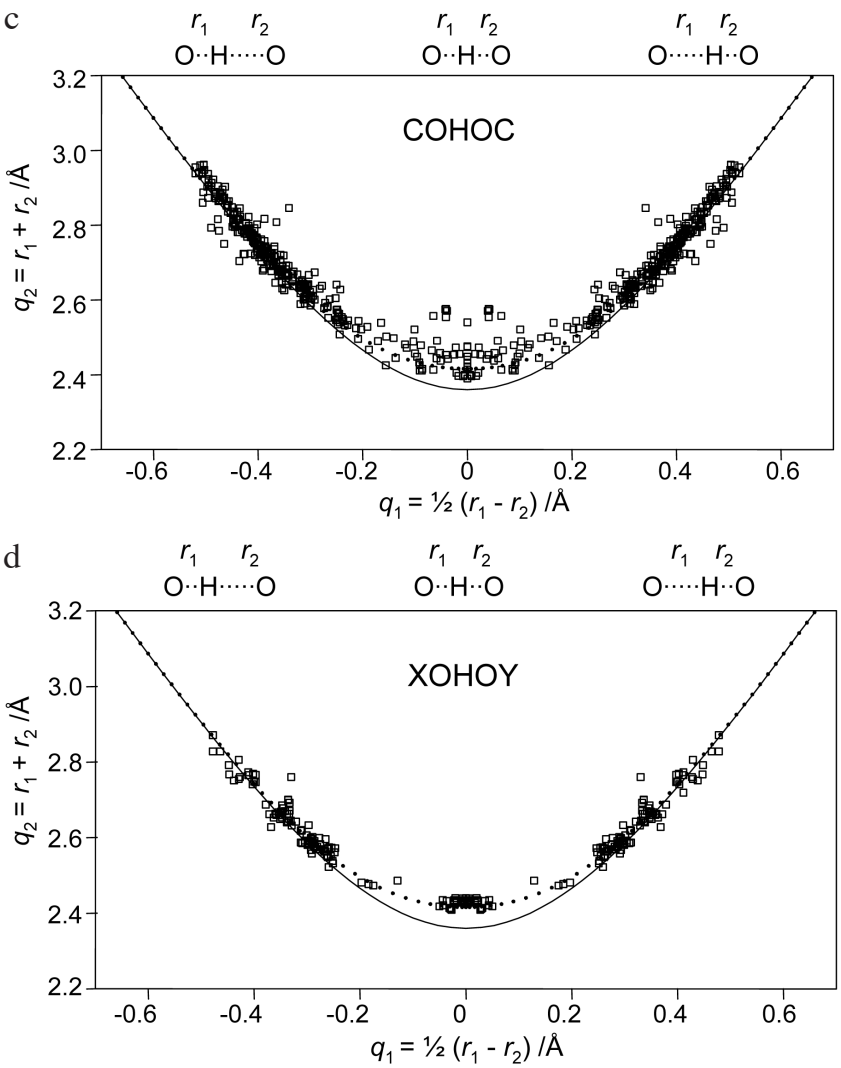

Fig. 2. *cont.* (c) XOHOY hydrogen bonds, where X, Y are both carbon atoms. (d) XOHOY hydrogen bonds, where X or Y or both are not carbon atoms. The correlation curves were calculated using the parameters listed in Table 1. For further description see text.

corresponding to the region of the symmetric hydrogen bonds around $q_1 = 0$ in Fig. 2d were derived mainly from urea–phosphoric acid complexes.

In order to reproduce the data points in the left and the right wing of the graph we had to reduce the parameter r^o from the value of 0.96 Å in Fig. 1 to the value of 0.93 Å, corresponding to a minimum O...O distance of 2.36 Å. Clearly, as noted previously for NHN- and OHN hydrogen bonds,[22,23] the experimental values of q_2 in the region of the correlation line are slightly larger than predicted for the equilibrium structures, a circumstance that is caused by QZPVE. This deviation was reproduced by the dotted line, calculated using eq 9 in connection with the parameters included in Table 1. Overall, the scattering of the data is substantially larger than in Fig. 1.

OHO Correlations of Compressed Ice

The QZPVE correction of eq 9 has been introduced into the valence bond order concept of hydrogen bonds in an empirical way.[22,23] We checked the literature for examples where the difference between classical and quantum-mechanical hydrogen bond geometries had been addressed previously; however, we only became aware of a paper of Benoit, Marx, and Parrinello,[31] who performed ab initio path integral Car–Parrinello molecular dynamics simulations on compressed ice VIII. Under pressure, the asymmetric OHO hydrogen bonds of ice are compressed, which reduces the O...O distances and shifts the proton to the hydrogen bond center. Once all protons are located in the center, the O...O distances can be further compressed. Benoit et al.[31] reported the OHO hydrogen bond geometries for the equilibrium or classical structures at 100 and 300 K, as well as the structures at 100 K where the proton is treated as a quantum particle. The geometric changes were achieved by confining a given number of water molecules in varying molecular volumes.

Whereas in the preceding cases mainly single hydrogen bonds were considered, water in ice is normally involved in four hydrogen bonds. As the valence bond order model refers to single hydrogen bonds, we wanted to check this concept for a large number of coupled OHO hydrogen bonds in compressed ice. Indeed, as shown in the following, the computed data of Benoit et al.[31] can be reproduced in a satisfactory way.

The data analysis obtained is depicted in Fig. 3. The solid curve 1 represents the computed data of a classical proton in compressed ice at 100 K, and the dotted curve 2 those of the quantum proton at 100 K. As a reference, we include the dashed curve 3, which represents the classical solid correlation curve of Fig. 2, valid at zero pressure. The experimental values for ice VIII are well located on these curves. When H is shifted to the hydrogen bond center via a pressure increase, the O... O distances shorten more rapidly as compared to zero pressure, leading to smaller values of q_2 for curve 1 as compared to curve 3. The effect is larger at low temperatures, as discussed before.[31] As in Fig. 2, the effect of

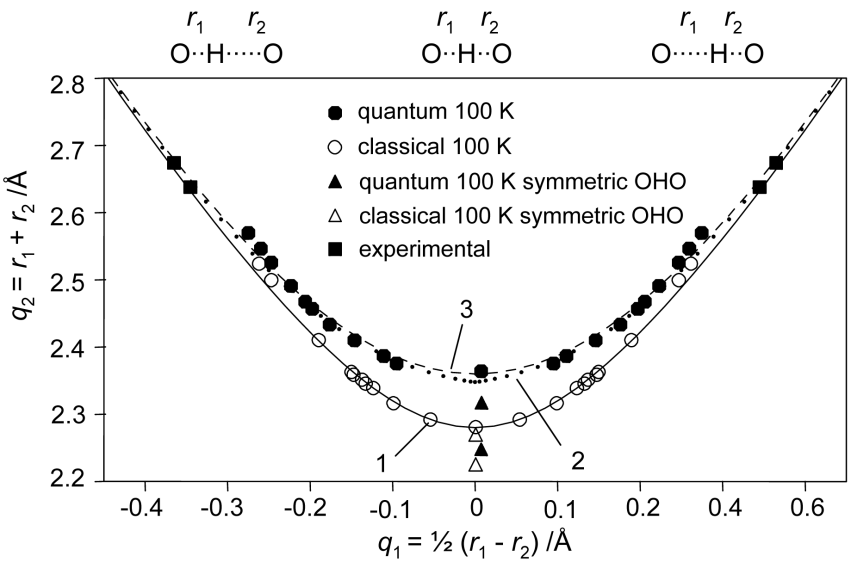

Fig. 3. Hydrogen bond correlation q_2 vs. q_1 of compressed ice VIII under pressure. The data points were taken from the paper of Benoit et al.[31] The correlation curves were calculated as described in Table 2. The solid curve 1 refers to the calculated equilibrium structures at 100 K; the dotted curve 2 includes the QZPVE correction. Dashed curve 3 corresponds to the calculated equilibrium structures at zero pressure.

the QZPVE correction leads again to an increase of the O...O distance because the quantum proton needs more space than a classical proton.[7] Thus, the valence bond order concept is able to describe also the large number of coupled hydrogen bonds in ice, with one exception: when ice has been symmetrized and H shifted to the H-bond center at $q_1 = 0$ by applying a given pressure, a further pressure increase only leads to a reduction of the O...O distance q_2, giving rise to a number of data points located on the ordinate as illustrated in Fig. 3.

Geometric H/D Isotope Effects

Our original goal for introducing the QZPVE correction was to describe H/D isotope effects on hydrogen bond geometries (GIE) as well as on related NMR parameters.[22,23] Whereas the *primary* geometric H/D isotope effect refers to the different values of the hydron coordinates q_1^H and q_1^D, the *secondary* geometric H/D isotope effect or Ubbelohde effect refers to the different values of the heavy atom coordinates q_2^H and q_2^D.[4] Unfortunately, the primary effect is very difficult to measure using neutron diffraction. For NHN and OHN hydrogen bonds, NMR methods have been proposed.[22,23]

Therefore, geometric data reported by Kiefer and Hynes[29] for an activated hydron transfer in OHO as compared to ODO bonds represent an excellent body of test data. The data were generated using an alternative model of hydron transfer along an arbitrary potential as a model for a hydrogen bond of intermediate strength. The data obtained are plotted in Fig. 4. They were well reproduced by the various curves defined in Table 1.

The calculated data points for OHO bonds indicate that the H transfer pathway strongly deviates from the classical solid correlation curve. In the beginning, a hydrogen bond compression occurs until a value of $q_2^H \approx 2.6$ Å is reached, where H is then transferred at fixed heavy atom positions. The transition state is located at $q_1^H = 0$. The dotted correlation line calculated as described in Table 1 reproduces well the H transfer pathway.

Kiefer and Hynes[29] find a different pathway for the deuteron in ODO bonds. This difference is highlighted in Figs. 4b and 4c where the *primary* GIE $\Delta q_1 = q_1^D - q_1^H$ and the *secondary* GIE $\Delta q_2 = q_2^D - q_2^H$ are plotted as a function of q_1^H. At the transition state $\Delta q_1 = 0$, i.e., both H and D are located in the hydrogen bond center where $q_1^H = q_1^D = 0$. By contrast, the value of Δq_2 is slightly negative, i.e., the hydrogen bond compression is somewhat larger for D than for H. Before reaching the H bond center, one observes that replacement of H by D increases q_2 and the absolute value of q_1. In other words, at a comparable reaction progress the ODO bond is longer and more asymmetric than the OHO bond.

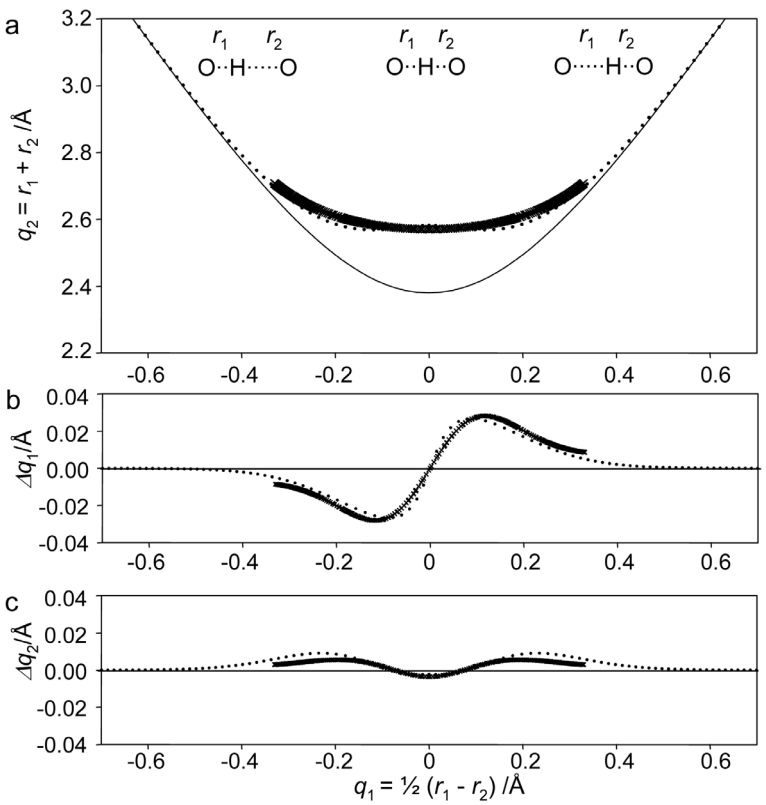

Fig. 4. Hydrogen bond correlation of a model OHO hydrogen bond. The data points were calculated by Kiefer and Hynes[29] using a multidimensional model potential. (a) q_2 vs. q_1. (b) *Primary* $\Delta q_1 = q_1^D - q_1^H$ and (c) *secondary* $\Delta q_2 = q_2^D - q_2^H$ geometric H/D isotope effects as a function of q_1^H. The correlation curves were calculated using the parameters listed in Table 1.

Similar effects have been observed previously for the stationary ground states of NHN and OHN hydrogen bonded model complexes.[4,5,20,22,23] Thus, whereas the reaction pathway (Fig. 4a) strongly deviates from the correlation curve, the geometric isotope effects are similar to those that will be obtained for stationary ground states.

^{1}H NMR Chemical Shift Correlations of OHO Hydrogen Bonds

Isolated protonated water dimer and neutral water clusters

We come now to the question of how the geometries of OHO hydrogen bonds are related to their ^{1}H NMR chemical shifts. Firstly, we will use a computational approach to this problem. In order to generate a chemical shift from a calculated chemical shielding value σ one needs to calculate a reference shielding value σ_{ref}. In this study we calculated the isotropic chemical shielding σ of isolated water as a reference; a value of 31.40 ppm was obtained. With respect to tetramethylsilane (TMS), monomeric gaseous water resonates at 0.73 ppm.[42] Thus, the chemical shift data reported were defined as

$$\delta = \sigma_{H_2O} - \sigma + 0.73 \text{ ppm} \qquad (13)$$

As the chemical shielding of a bare proton is zero, its chemical shift with respect to TMS is then 32.13 ppm.

The results of the chemical shift calculations performed on the protonated water dimer and on the water clusters $(H_2O)_n$, n = 2 to 16 confined in C180, are depicted in Fig. 5a. These data served to determine the parameters of the different correlation curves. These parameters are included in Table 1.

In a first step, we calculated the chemical shift of the protonated water dimer that exhibits the shortest hydrogen bond with q_2 = 2.38 Å. We obtain a value of 20.93 ppm with respect to TMS. This value is smaller than the value of 23.1 ppm calculated by Janoschek.[42] It coincides, however, with the value reported by Del Bene et al.[39] We then calculated the shielding parameters of the protonated water dimer along the classical q_2 vs. q_1 correlation curve of Fig. 1. The data are depicted on the upper left side of the graph as solid circles, which are represented by the classical correlation curve 1 calculated using eq 11. At very large values of q_2, corresponding to the isolated Eigen cation H_3O^+, we obtain a chemical shift of 7.9 ppm, which is close to the value of 8.27 ppm calculated previously.[42] The data of the right upper curve 2 are discussed below.

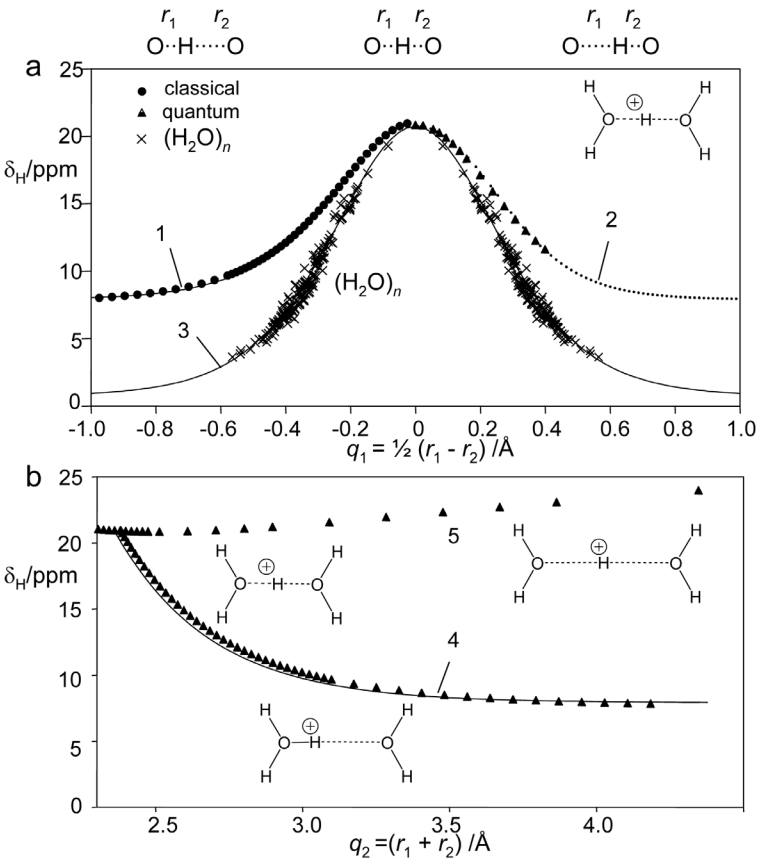

Fig. 5. (a) Calculated ^{1}H chemical shifts of the protonated Zundel cation $H_5O_2^+$ (filled symbols) and of water clusters $(H_2O)_n$, n = 2 to 16 confined in fullerene C180, as a function of q_1. Curve 1 and data points: $H_5O_2^+$ exhibiting the classical equilibrium hydrogen bond geometries of the correlation curve in Fig. 1. Curve 2 and data points: $H_5O_2^+$ exhibiting the corrected equilibrium hydrogen bond geometries of the dotted correlation curve in Fig. 1 where QZPVE are taken into account. Curve 3 and data points: values of water clusters in C180 calculated in this study for the geometries calculated by Wang et al.[40] (b) Curve 4 and data points of $H_5O_2^+$: same as curve 1, but as a function of q_2. Data points of curve 5: values calculated for the symmetric $H_5O_2^+$ Zundel cation as a function of q_2. The correlation curves were calculated as described in Table 1.

In the next step, we calculated the chemical shifts of the neutral water clusters in C180 giving rise to the crosses in Fig. 5. The data points are well located on the correlation curve 3 calculated for a classical proton using eq 11. Whereas the maximum chemical shift is similar to the one found for the Zundel cation, the left and right wings join the value of 0.73 ppm of isolated water. A remarkably large spread of chemical shifts between 3 and 19 ppm is observed for the confined water clusters. The above-mentioned very strong hydrogen bond in $(H_2O)_{16}$ gives rise to the largest low-field shift of 19.3 ppm.

These data indicate a large effect of the chemical environment on the chemical shifts, especially in the regime of weak hydrogen bonds. By contrast, in the strong hydrogen bond regime the effects are much less pronounced. Preliminary calculations of the deprotonated water and formic acid dimers indicate maximum chemical shift values that are about 1 ppm smaller than those of the Zundel cation.

We wanted then to estimate the influence of the QZPVE correction on the ^{1}H chemical shifts. The correct way would normally be to calculate the nuclear wave functions in anharmonic approximation[43] as well as the complete chemical shielding surface in order to obtain the vibrationally averaged chemical shifts. Here, we used the empirical procedure described in the Theoretical Section and in the discussion of Fig. 1. Thus, we repeated the chemical shift calculation of the protonated water dimer for the corrected hydrogen bond geometries represented by the dotted line in Fig. 1. We obtained the data points depicted on the right upper side of Fig. 5. We were quite astonished to find almost no difference between the chemical shifts of the classical and the quantum-mechanical proton as illustrated in Fig. 5a, in spite of the larger O...O distance in the latter case. Thus, curve 2, which was calculated using eq 12 and the parameters listed in Table 1, almost coincides with the classical curve 1.

We were suspicious about this effect and calculated the GIAO chemical shielding tensor of the hydrogen-bonded proton in the protonated water dimer where we confined the proton in the hydrogen bond center, but where the H...O distances corresponding to half of the values of q_2 were systematically changed between 2.2 and 5 Å. The calculated isotropic chemical shifts are depicted in Fig. 5b (upper data series). The dependence of the chemical shifts on q_2 is very small. When the O...O distance is increased, the chemical shift slightly decreases and then increases again. As the main effect of the quantum zero-point motion of the proton in a symmetric hydrogen bond is to increase the O...O distance, it becomes clear why the QZPVE correction on the ^{1}H chemical shifts is small and negligible.

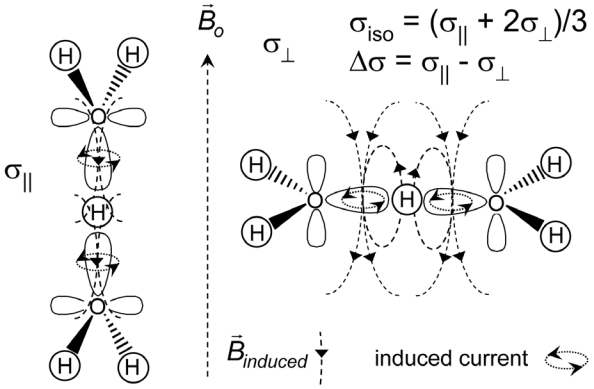

Fig. 6. NMR chemical shielding values σ of the protonated water dimer at different orientations in the applied magnetic field B_o. $B_{induced}$: induced magnetic field arising from the Lorentz force. For further description see text.

The little dependence of the chemical shifts with q_2 can be rationalized by having a closer look at the elements σ_{XX}, σ_{YY}, and σ_{ZZ} of the calculated GIAO chemical shielding tensor. The difference between σ_{XX} and σ_{YY} is small and, moreover, averaged by fast rotations of the water molecules along the molecular Z-axis. In good approximation, the tensor is axially symmetric, and

$$\sigma_{||} = \sigma_{ZZ},\ \sigma_\perp = (\sigma_{XX}+\sigma_{YY})/2,\ \Delta\sigma = \sigma_{||} - \sigma_\perp.$$
$$\sigma_{iso} = (\sigma_{||} + 2\sigma_\perp)/3 \qquad (14)$$

The situation is illustrated schematically in Fig. 6. The effective magnetic field at the nucleus is $B_{eff} = B_o - B_{induced} = B_o(1 - \sigma)$. $B_{induced}$ is created by electrical currents in the electronic system induced by the applied magnetic field B_o via the Lorentz force. The shielding ($\sigma_{||}$) is large when the molecular axis is parallel to B_o because the induced field weakens the applied field. By contrast, the shielding ($\sigma_\perp$) is small, as the molecular axis is perpendicular to B_o: here, the effective magnetic field is much less weakened or may even be stronger than the applied field, as the induced field is parallel to the latter. Because of the factor of 2 in eq 14, this deshielding

Table 3. Calculated shielding and chemical shift values of the symmetric protonated water dimer

q_2 /Å	σ_{iso}/ppm	δ/ppm	$\sigma_{||}$ /ppm	$\sigma_\perp$/ppm	Δσ/ppm
2.22	10.89	21.26	50.45	–8.89	59.33
2.36	11.20	20.95	46.05	–6.23	52.28
2.51	11.29	20.86	41.33	–3.74	45.07
2.61	11.25	20.90	38.70	–2.47	41.17
2.80	11.06	21.09	34.11	–0.47	34.58
2.90	10.92	21.22	32.11	0.33	31.79
3.29	10.19	21.95	25.54	2.52	23.01
3.48	9.81	22.34	22.97	3.23	19.74
4.35	8.17	23.00	15.19	4.66	10.53
4.83	7.29	24.86	12.44	4.72	7.73
5.80	5.16	26.99	8.20	3.64	4.55
∞	0	32.14	0	0	0

dominates the isotropic value. Table 3 contains a selection of chemical shielding values calculated for different O...O distances. A more complete data set is included in Table S4 of the Supplementary Information.

At small O...O distances the proton is deshielded by the neighboring effect of the oxygen lone pairs, as illustrated in Fig. 6. The chemical shift anisotropy is very large. This effect is attenuated when the O...O distance increases, i.e., the isotropic shielding increases slightly and the chemical shift becomes smaller. However, at very large O...O distances a bare proton is left, exhibiting zero shielding, i.e., a chemical shift of 32.13 ppm, and the anisotropy is zero. These competing factors, the deshielding in the bare proton at large O...O distances and the deshielding by the oxygen lone pairs at small O...O distances, lead then to the flat dependence of the chemical shift with the O...O distance.

Solids containing OHO hydrogen bonds

Let us analyze now solids exhibiting OHO hydrogen bonds for which both the neutron crystallographic data as well as the solid state ^{1}H NMR chemical shifts are known. Most data were taken from refs 24 and 27, as described in the Supplementary material. The known data are depicted in Fig. 7. They all refer to OHO hydrogen bonds bound to adjacent carbon atoms. At first sight, the scattering of the data seems to be very large. A closer look, however, reveals a different behavior of aliphatic hydroxyl groups (alcoholic groups, filled circles) bound to saturated carbon atoms, i.e., XCR_2–OH, and hydroxyl groups bound to unsaturated carbon atoms, i.e., X = CR–OH (open squares). The latter can be carboxylic acids, phenols, or enols. The curves in Fig. 7 were calculated using the parameters included in Table 1. On the right side are shown the dotted curves 1 and 2, which were calculated taking QZPVE into account by using eq 12. For the free aliphatic OH groups we assumed as limiting value for δ_{OH}^{o} the water gas phase value of 0.73 ppm, which is also close to the value found for the water monomer in CCl_4[44] (Table 4). For the OH groups bound to unsaturated carbon we used the limiting value $\delta_{OH}^{o} = 6$ ppm, which was estimated from the calculated chemical shift of the formic acid monomer (Table 4). The excess term Δ_H* exhibits a large margin of error as illustrated by the dotted lines 5 and 6. Line 5 represents the value of 21.3 ppm found for the protonated water dimer in polar aprotic solution reported by Golubev.[45] Line 6 corresponds to the largest value of 19.6 ppm found for the solid state. Such deviations from the maximum value may arise from the presence of fast proton transfers between two states which exhibit larger O...O distances than the minimum distance.

On the left side of Fig. 7 are depicted dashed curves 3 and 4, which were calculated using

$$\delta_H = 0.73 + 19.8 \exp(-6.2\, q_1^2) \text{ for } XCR_2 - OH$$
$$\delta_H = 6 + 14.5 \exp(-6.2\, q_1^2) \text{ for } X = CR - OH. \quad (15)$$

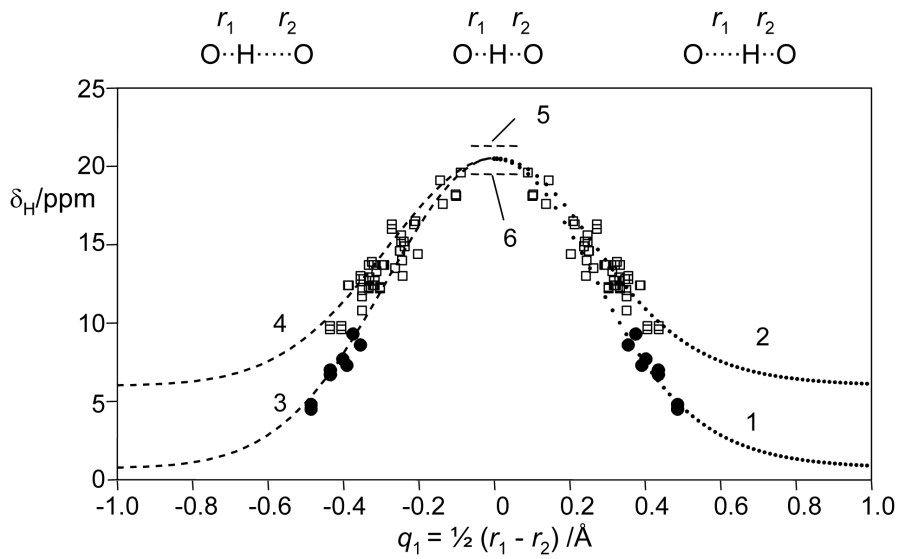

Fig. 7. Room-temperature solid state ^{1}H NMR chemical shifts[24,27,28] of solids containing COHOC hydrogen bonds as a function of the hydrogen bond coordinate q_1 obtained from low-temperature neutron structures in the Cambridge Structural Database. Filled circles: aliphatic OH groups; open squares: OH groups bound to unsaturated carbon, e.g., carboxylic acids, phenols, etc. The dotted curves 1 and 2 were calculated as described in Table 2, taking QZPVE into account. The dashed curves 3 and 4 were calculated using eq 15. Curve 5 represents the chemical shift of the protonated water dimer in solution.[45] Curve 6 represents the lower limit of the maximum chemical shift estimated from the experimental data.

Table 4. 1H NMR chemical shielding and shifts of various OH groups

system	environment	method	r(OH)/Å	σ(OH)/ppm	δ(TMS)/ppm
H_2O monomer	gas	calculated	0.963[39]	31.4175	0.73[42]
H_2O monomer	benzene	experimental			0.4/30ºC[44]
H_2O monomer	CCl_4	experimental			1.2/30ºC[44]
water	liquid	experimental			4.8/25ºC[44]
Formic acid	gas	calculated		26.2619[a]	5.9[a]
$H_2OH^+OH_2$	gas	calculated	1.39[38,39]		20.93[39]
H^+	gas	calculated		0	32.14
H_3OH^+	gas	calculated			8.27[42]
H_3OH^+	gas	calculated	0.9779		7.54[a]
$H_2OH^+OH_2$ $C_8H_{17}SO_3^-$	CDF_3/CDF_2Cl	experimental			21.3[45]

[a]This work.

All lines reproduce very well the experimental data. Equation 15 has the advantage that H-bond geometries can be obtained very easily.

Average chemical shifts of water clusters

The study of water clusters in inorganic[46] and organic[47] solid model pores using solid state ^{1}H and ^{2}H NMR spectroscopy is a matter of current interest. The problem is that water is highly mobile in such systems, leading to a fast rearrangement of hydrogen bonds. Therefore, it will be difficult to determine experimentally chemical shifts of individual hydrogen bonds as calculated for those of the water clusters in C180 depicted by the crosses in Fig. 5a. For this reason, we have calculated the averaged chemical shifts for these data.

Let us first discuss the structure of the clusters. The ratio between the bonded and free OH groups n_b/n_f is first depicted in Fig. 8a. This ratio starts at 0 for the water monomer, goes to 1/3 for the water dimer, and then to 1 for the cyclic ring structures of the trimers, tetramers, and pentamers. The hexamer exhibits already a cage structure. For these cage structures n_b/n_f is close to 3, independent of the number of water molecules in the cage. However, we note that these structures are partially enforced by the surrounding C180. Furthermore, all cages studied exhibit in crude approximation a spherical structure, with no water inside the cages.

In Fig. 8b the calculated average chemical shifts of the clusters are depicted. Although there is no direct exchange process that interconverts the free OH groups

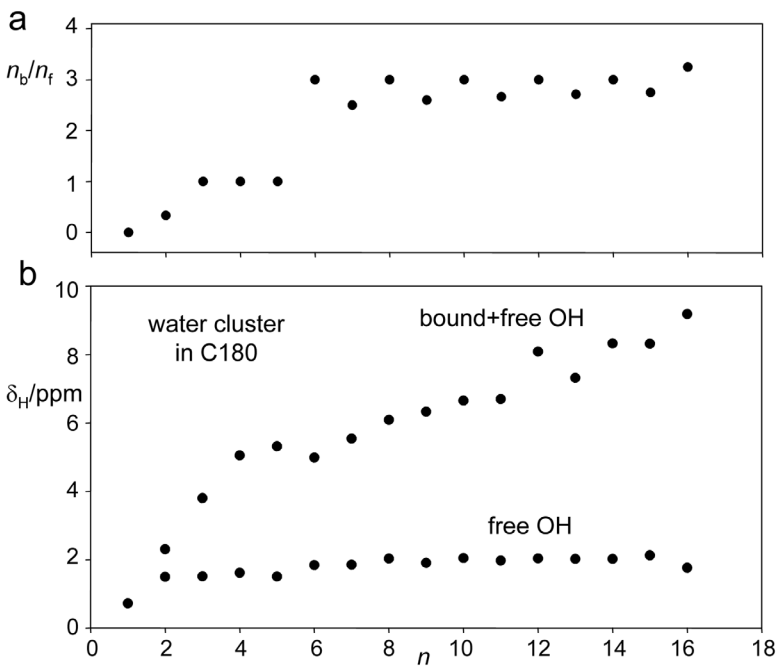

Fig. 8. (a) Ratio of hydrogen-bonded OH groups to non-hydrogen-bonded OH groups of water clusters $(H_2O)_n$, n = 2 to 16 confined in fullerene C180,[40] as a function of n. (b) Average ^{1}H chemical shifts calculated in this study of all OH groups (upper data points) and of the free OH groups (lower data points).

without exchange with hydrogen-bonded groups, it is interesting to have a look at the average chemical shift of the free OH groups. As mentioned above, the value of the water monomer is 0.73 ppm. The value of the free OH group of the water donor in the dimer is almost the same (0.78 ppm). By contrast, the value of the free OH groups of the acceptor water is shifted downfield to about 1.8 ppm. Thus, the average value of the free OH groups is about 1.5 ppm. This value increases only slightly for cyclic clusters, but reaches a value around 2 ppm for the cages with $n \geq 6$, as indicated by the lower body of data in Fig. 8.

The average chemical shifts of all OH groups are depicted in the upper curve of Fig. 8b. A strong low-field shift is obtained for the dimer to 2.3 ppm, and for the cyclic trimer and tetramer to about 3.8 and 5 ppm. Then, a saturation occurs and the value in the cyclic pentamer is only slightly shifted to 5.3 ppm. However, when a cage is formed in the hexamer, a slight drop is observed although the number of bound OH groups is strongly increased, and although the average value of the free OH groups is almost not altered. This effect arises from the circumstance that the hydrogen bonds are weaker in the cage hexamer than in the cyclic pentamer. However, they become stronger again with an increasing number of water molecules in the cage. At $n = 11$ the effect of the confinement of the surrounding C180 leads to a strong compression of the OHO hydrogen bonds, leading to strong average low field shifts to 9 ppm and higher.

We conclude that if one wants to estimate the number of free to bound OH groups from average ^{1}H NMR chemical shifts of water clusters, one should take into account that the free OH groups of the clusters are shifted about 1 to 1.5 ppm to lower field as compared to the water monomer. Furthermore, values of average chemical shifts of about 6 ppm or higher may be possible.

OHO hydrogen bonds in organic solvents

The next question that arises is whether the results depicted in Figs. 7 and 8 are valid not only for the solid state but can also be used in order to derive OHO hydrogen-bond geometries from ^{1}H NMR chemical shift values in solution.

In order to deal with this question let us first discuss the dashed horizontal line 5 in Fig. 7. The line represents the chemical shift value of $\delta_H = 21.3$ ppm[45] for the inner proton of the protonated water dimer. This species was observed in the slow hydrogen bond and proton exchange regime at 90 K using a freon mixture CDF_3/CDF_2Cl as solvent. As the outer protons were found to resonate around 6 ppm, it was argued that they all form hydrogen bonds with $C_8H_{17}SO_3^-$ added as counter anion.

The value of $\delta_H = 21.3$ ppm is in good agreement with the calculated values of the protonated water dimer (Fig. 5a). This agreement implies a high symmetry of the cation in solution, which may be caused by the placement of the two anions on both sides of the cation. The value also indicates that the local environment of the cation has a minor influence on δ_H. This is in agreement with the little influence of the O...O distance on δ_H according to Fig. 5b. By contrast, a larger influence of the environment can be expected for free or weakly hydrogen-bonded OH groups as demonstrated by the following.

Nakahara and Wakai[44] have measured ^{1}H chemical shifts of water in organic solvents. At low concentrations and room temperature, signals at higher field were observed, which can be assigned to the water monomer, for example 0.6 ppm and 1 ppm for benzene and CCl_4 as solvents. By contrast, for cyclohexane and chloroform values of about 1.5 ppm are observed. In the latter case, the value increases to about 2 ppm when lowering temperature. This temperature decrease leads to a phase separation due to the reduced water solubility; water droplets appear which are still mobile for some time, exhibiting values between 4.5 and 6 ppm depending on the solvent and the temperature. These results indicate that some caution has to be taken when using eq 15 for polar solvents; one needs to take into account that the value of the fictive free OH group might be shifted by the order of 1 ppm to low field. This has been discussed in a previous paper on OHN hydrogen bonds, where such a difference was observed for a chemical shift correlation curve for the free neutral OH group.[22]

In conclusion, the maximum ^{1}H chemical shift of the strongest OHO hydrogen bond may vary between 20 and 21.5 ppm, where the environment could play a role.

Liquid water simulations

The structure of liquid water is one of the topics of great current interest. Using high-level ab initio calculations of the pair potential of the water dimer followed by molecular dynamics calculations, it has become possible to obtain atom–atom radial distribution functions as well as thermodynamic quantities.[48] Experimental neutron diffraction studies provide atom–atom radial distribution functions. Thus, it was found that the O...O radial distribution function exhibits a peak for the nearest neighbor at 2.8 Å, exhibiting a width of about ±0.2 Å.[49]

In this context we would like to discuss a recent computational study of Murakhtina et al.[32] of the ^{1}H NMR

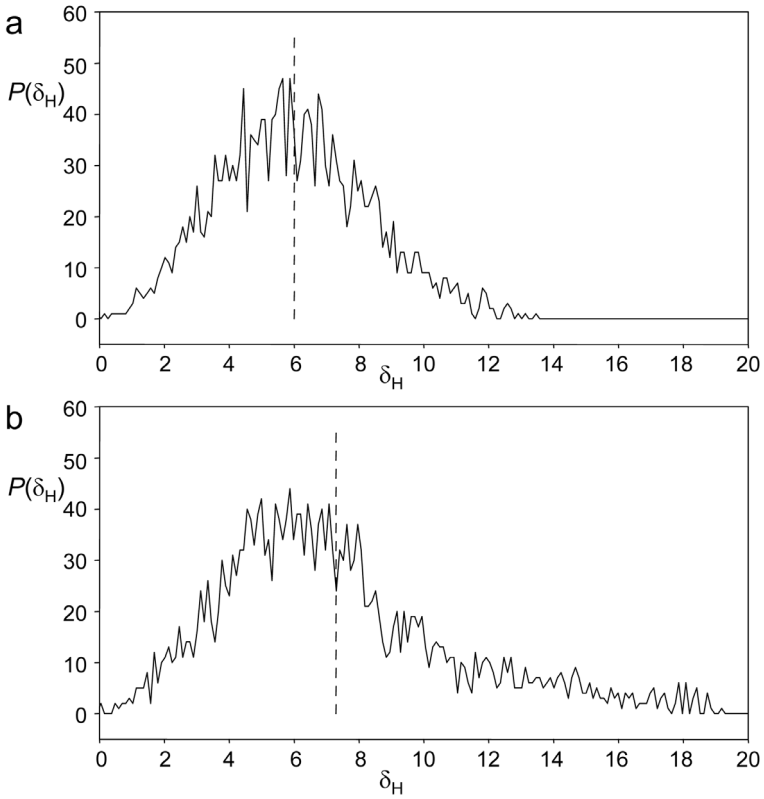

Fig. 9. (a) Relative probabilities $P(\delta)$ of finding a given ^{1}H chemical shift of OH groups in pure water (a) and in water containing 4.9 M HCl (b). The values of $P(\delta)$ were calculated using Car–Parrinello molecular dynamics simulations and fully periodic NMR chemical shift calculations by Murakhtina et al.[32] The dashed vertical lines represent the average chemical shift which can be compared to the experiment.

chemical shift distribution of pure water and of aqueous hydrogen chloride solutions based on Car–Parrinello molecular dynamics simulations and fully periodic NMR chemical shift calculations. Some of their results are depicted in Fig. 9. An average chemical shift of about 6 ppm is obtained at 300 K, which is only about 1 ppm larger than the experimental values. According to Figs. 7 and 2a, the average shift corresponds to a value of $q_1 = 0.55$ Å and hence of $q_2 = 2.8$ Å, which is close to the O...O distance in the bulk liquid. Even more important is the finding of a very broad distribution of chemical shift values in the range between 2 and 10 ppm. According to Fig. 7, this range corresponds to a distribution of values of q_1 between 0.35 and 0.6 Å, and according to Fig. 2a to values of q_2 between 2.6 and 3.1 Å. This is in excellent agreement with the above-mentioned diffraction studies.

Murakhtina et al.[32] also performed calculations of ^{1}H NMR chemical shifts for 2.9 and 4.9 M aqueous HCl solutions. The result is depicted in Fig. 9b. The authors notice an increase of the probability to find chemical shift values above 10 ppm, up to 19 ppm. Values above 20 ppm, which would be characteristic for symmetric Zundel cation, are not observed. Thus, the authors argue that the protonated water molecules exhibit a structure somewhere between an asymmetric Zundel cation and an Eigen cation. The chemical shifts of water OH groups bound to chlorine are found around 3 ppm, and do not give rise to a separate peak in the distribution.

The results discussed above indicate that it is difficult to assign a unique ^{1}H NMR chemical shift to bound water, which could then be used together with the value of about 2 ppm of non-hydrogen bonded or "free" water OH groups to calculate the fraction of the latter from the average water chemical shift, which exhibits a strong temperature dependence. Thus, it could be that there is both a larger number of free OH groups—as proposed on the basis of X-ray absorption spectroscopy and X-ray Raman scattering[50]—as well as a larger number of stronger hydrogen bonds resonating well above 6 ppm than one may have anticipated before. Thus, the explanation of the observed temperature dependence of the

^{1}H NMR chemical shifts of water and water clusters is still challenging.

CONCLUSIONS

The conclusions of this study can be summarized as follows.

(1) Neglecting the ellipsoidal shape of the proton in the hydrogen bond (Scheme 1), the correlation between the two distances r_1 and r_2 of OHO hydrogen bonds or between the proton or heavy atom coordinates q_1 and q_2 (Scheme 1) can be reproduced by ab initio or DFT calculations of series of equilibrium or classical structures. As examples, hydrogen bond geometries of various water clusters and of the Zundel cation were considered (Fig. 1). Water clusters confined in the fullerene C180 can exhibit a large variation of O...O distances.[40] Different levels of calculation do not produce substantial deviations from the geometric hydrogen bond correlations but, rather, lead to shift along the correlation curves.

(2) Quantum zero-point vibrational effects (QZPVE) on the average hydrogen bond coordinates q_1 and q_2 can be taken into account using an empirical system-dependent correction term. For normal asymmetric OHO hydrogen bonds that are characterized by averaged hydrogen bond coordinates, the correction term can be obtained from neutron structures. Proton tautomerism leads to deviations from the correlation curves. The correction terms could reproduce quantum effects on the symmetrization of ice under pressure (Fig. 3) calculated by Benoit et al.[31] The term also allows one to describe H/D isotope effects on hydrogen bond geometries along the proton reaction pathway in strong OHO hydrogen bonds exhibiting a double-well potential, after suitable parametrization (Fig. 4). Whereas H and D exhibit the masses 1 and 2, the equilibrium structures are valid for a hypothetical hydrogen isotope of infinite mass. For symmetric O...O hydrogen bonds, where the hydrogen isotope is located in the hydrogen bond center, the O...O distance increases with decreasing mass because of the increase of the width of the hydrogen wave function in the vibrational ground state. For asymmetric configurations, reducing the mass of the hydrogen isotope leads to a decrease of the O...O distances (*secondary geometric isotope effect*) and to a shift of the hydrogen isotope towards the hydrogen bond center (*primary geometric isotope effect*) (Fig. 4).

(3) ^{1}H chemical shift calculations of water clusters $(H_2O)_n$, n = 2 to 16 based on geometries calculated for these clusters using DFT methods by Wang et al.[40] allowed us to establish a relation between these shifts and the hydrogen bond coordinates (Fig. 5). Additional calculations were performed on the Zundel cation that provided interesting insights. Calculations along the classical and the quantum-corrected q_1 vs. q_2 correlation curves showed almost no difference (Fig. 5, curves 1 and 2), indicating that QZPVE do not influence the chemical shift correlation curve substantially. As this result was suspicious, chemical shifts of the symmetric Zundel cation were calculated as a function of q_2, i.e., the O...O distance. Only a very small dependence was observed around 2.4 Å, exhibiting a shallow minimum around 2.6 Å. This result arises from the fact that at infinite O...O distance the naked proton does not exhibit any shielding (32.13 ppm vs. TMS); on the other hand, when the O...O distances are decreased below 2.4 Å the proton signal is again shifted to low field because of the increasing neighboring effects of the oxygen lone pairs that increase the chemical shielding anisotropy. Both deshielding processes lead to the little dependence of the ^{1}H chemical shifts on the O...O distances around $q_1 = 0$, and hence QZPVE, which slightly increases these distances, is not operative. Finally, Fig. 5 indicates that in the strong hydrogen bond regime the effects of the varying chemical structures and environments are not very pronounced, in contrast to the weak hydrogen bond limit, where the chemical shifts of free OH groups strongly depend on the chemistry and the environment.

(4) Using these results, experimental room-temperature ^{1}H chemical shifts of OHO hydrogen-bonded solids for which low-temperature neutron structures are contained in the Cambridge Structural Database were reanalyzed (Fig. 7). It was clearly shown that OH groups bound to unsaturated and saturated carbon exhibit chemical shift vs. q_1 correlation curves that differ in the weak hydrogen bond regime, but that coincide in the strong hydrogen bond regime. A simple equation relating chemical shifts and q_1 was derived (eq 15), whose parameters are system dependent.

(5) Using eq 15, average ^{1}H chemical shifts of water clusters were calculated valid for the case of fast hydrogen bond exchange regime. The average chemical shift of the free OH groups was found to be downfield-shifted by 1 ppm from the value of the free water monomer. Moreover, in larger water clusters confined in organic pores, hydrogen bond compression can occur. Thus, average chemical shifts between 5 and 7 ppm may result even in the presence of 25% free OH groups. However, caution

needs to be taken if eq is applied for liquid solution in the area of week hydrogen bonds. According to Nakahara and Wakai,[44] the solvent can influence the shifts of the free OH groups.

(6) Calculations of Murakhtina et al.[32] of the chemical shift distribution in pure water indicate a broad range of values between 2 and 10 ppm, which are averaged by hydrogen bond and proton exchange. Using eq 15 a distribution of O...O distances of 2.8 ± 0.2 Å can be estimated, which is in agreement with the width of the first-shell O...O radial distribution function.[48,49] This range is similar to the range of O...O distances in the water clusters confined in C180.[40] From these consideration it also follows that the average ^{1}H NMR chemical shifts cannot be explained in terms of a simple equilibrium between free and bound OH groups. Thus, it could be that both the number of stronger hydrogen bonds and of weaker or free OH groups is larger than a simple equilibrium would predict. A major fraction of free OH groups had been postulated previously by Wernet et al. using X-ray absorption and diffraction studies,[50] a possibility which is currently discussed.[51]

As a final conclusion, we note that the technique of hydrogen bond and NMR correlations provides a framework for interpretations which may have interesting applications and which may lead to new questions and answers.

Acknowledgments. The authors would like to thank Professor Dominique Marx, Bochum, Professor Casey Hynes, Paris and Boulder, Colorado, Dr. Phil Kiefer, Boulder, Colorado, and Dr. Daniel Sebastiani, Mainz, for stimulating discussions and for providing us with numerical data on which Figs. 3, 4, and 9 are based. This work has been supported by the Deutsche Forschungsgemeinschaft, the Fonds der Chemischen Industrie, Frankfurt.

Supporting Information Available: DOI: 10.1560/IJC.49.2.S1 The data points from which Figs. 1 to 5 and 7 to 9 are constructed are available in numerical form in Tables S1 to S6.

REFERENCES AND NOTES

(1) Jeffrey, G.A.; Saenger, W. *Hydrogen Bonding in Biological Structures*; Springer: Berlin, 1991.

(2) (a) Roberts, J.E.; Harbison, G.S.; Munowitz, M.G.; Herzfeld, J.; Griffin, R.G. *J. Am. Chem. Soc.* **1987**, *109*, 4163–4169. (b) Tekely, P.; Montigny, F.; Canet, F.; Delpuech, J.J. *Chem. Phys. Lett.* **1990**, *175*, 401–406. (c) Munowitz, M.G.; Griffin, R.G. *J. Chem. Phys.* **1982**, *76*, 2848–2858. (d) Munowitz, M.G.; Aue, W.P.; Griffin, R.G. *J . Chem. Phys.* **1982**, *77*, 1686–1689.

(3) Hoelger, C.G.; Limbach, H.H. *J. Phys. Chem.* **1994**, *98*, 11803–11810.

(4) Benedict, H.; Limbach, H.H.; Wehlan, M.; Fehlhammer, W.P.; Golubev, N.S.; Janoschek, R. *J. Am. Chem. Soc.* **1998**, *120*, 2939–2950.

(5) Lorente, P.; Shenderovich, I.G.; Buntkowsky, G.; Golubev, N.S.; Denisov, G.S.; Limbach, H.H. *Magn. Res. Chem.* **2001**, *39*, S18–S29.

(6) Sack, I.; Goldbourt, A.; Vega, S.; Buntkowsky, G. *J. Magn. Res.* **1999**, *138*, 54–65.

(7) (a) Benoit, M.; Marx, D. *ChemPhysChem* **2005**, *6*, 1738–1741. (b) Marx, D. *ChemPhysChem* **2006**, *7*, 1848–1870. Addendum: *ChemPhysChem* **2007**, *8*, 209–210.

(8) Steiner, T.J.; Saenger, W. *Acta Crystallogr.* **1994**, *B50*, 348–357.

(9) Steiner, T.J. *J. Chem. Soc., Chem. Commun.* **1995**, 1331–1332.

(10) Steiner, T.J. *J. Phys. Chem. A.* **1998**, *102*, 7041–7052.

(11) Gilli, P.; Bertolasi, V.; Ferretti, V.; Gilli, G. *J. Am. Chem. Soc.* **1994**, *116*, 909–915.

(12) Pauling, L. *J. Am. Chem. Soc.* **1947**, *69*, 542–553.

(13) Brown, I.D. *Acta Crystallogr.* **1992**, *B48*, 553–572.

(14) Bürgi, H.B.; Dunitz, J.D. *Acc. Chem. Res.* **1983**, *16*, 153–161.

(15) Truhlar, D.G. *J. Am. Chem. Soc.* **1972**, *94*, 7584–7586.

(16) Agmon, N. *Chem. Phys. Lett.* **1977**, *45*, 343–345.

(17) Lapid, H.; Agmon, N.; Petersen, M.K.; Voth, G.A. *J. Chem. Phys.* **2005**, *122*, 014506-1–014506-11.

(18) Ramos, M.; Alkorta, I.; Elguero, J.; Golubev, N.S.; Denisov, G.S.; Benedict, H.; Limbach, H.H. *J. Phys. Chem. A* **1997**, *101*, 9791–9800.

(19) Picazo, O.; Alkorta, I., Elguero, J. *J. Org. Chem.* **2003**, *68*, 7485–7489.

(20) (a) Shenderovich, I.G.; Smirnov, S.N.; Denisov, G.S.; Gindin, V.A.; Golubev, N.S.; Dunger, A.; Reibke, R.; Kirpekar, S.; Malkina, O.L.; Limbach, H.H. *Ber. Bunsenges. Phys. Chem.* **1998**, *102*, 422–428. (b) Shenderovich, I.G.; Tolstoy, P.M.; Golubev, N.S.; Smirnov, S.N.; Denisov, G.S.; Limbach, H.H. *J. Am. Chem. Soc.* **2003**, *125*, 11710–11720.

(21) Vener, M.V.; Manaev, A.V.; Egorova, A.N.; Tsirelson, V.G. *J. Phys. Chem. A* **2007**, *111*, 1155–1162.

(22) Limbach, H.H.; Pietrzak, M.; Benedict, H.; Tolstoy, P.M.; Golubev, N.S.; Denisov, G.S. *J. Mol. Struct.* **2004**, *706*, 115–119.

(23) Limbach, H.H.; Pietrzak, M.; Sharif, S.; Tolstoy, P.M.; Shenderovich, I.G.; Smirnov, S.N.; Golubev, N.S.; Denisov, G.S. *Chem. Eur. J.* **2004**, *10*, 5195–5204.

(24) (a) Sternberg, U.; Brunner, E.L. *J. Magn. Res. A* **1994**, *108*, 142–150. (b) Brunner, E.; Sternberg, U. *J. Progr. NMR Spectrosc.* **1998**, *32*, 21–57.

(25) McDermott, A.; Ridenour, C.F. *Proton Chemical Shift Measurements in Biological Solids*. In *Encyclopedia of NMR*; Wiley: Sussex, UK, 1996; pp 3820–3825.

(26) Mildvan, T.K.; Harris, A.S. *Proteins: Struc. Funct., Genet.* **1999**, *35*, 275–282.

(27) Harris, R.K.; Jackson, P.; Merwin, L.H.; Say, B.J.;

Hägele, G. *Chem. Soc. Faraday Trans. 1* **1988**, *84*, 3649–3672.
(28) Emmler, T.; Gieschler, S.; Limbach, H.H.; Buntkowsky, G. *J. Mol. Struct.* **2004**, *700,* 29–38.
(29) Kiefer, P.M; Hynes, J.T. To be submitted for publication.
(30) (a) Kiefer, P.M; Hynes, J.T. *J. Phys. Chem. A* **2002**, *106*, 1834–1849. (b) Kiefer, P.M; Hynes, J.T. *J. Phys. Chem. A* **2002**, *106*, 1850–1861. (c) Kiefer, P.M; Hynes, J.T. *J. Phys. Chem. A* **2003**, *107*, 9022–9039.
(31) Benoit, M.; Marx, D.; Parrinello, M. *Nature* **1998**, *392*, 258–261.
(32) Murakhtina, T.; Heuft, J.; Meijer, E.J.; Sebastiani, D. *ChemPhysChem* **2006**, *7*, 2578–2584.
(33) Ubbelohde, A.R.; Gallagher, K.J. *Acta Crystallogr.* **1955**, *8*, 71–83.
(34) Benedict, H.; Shenderovich, I.G.; Malkina, O.L.; Malkin, V.G.; Denisov, G.S.; Golubev, N.S.; Limbach, H.H. *J. Am. Chem. Soc.* **2000**, *122*, 1979–1988.
(35) Frisch, M.J., et al. *Gaussian 98, Revision A.11*. (Gaussian, Inc., Pittsburgh PA, 2001). For the full Reference see Supporting Information.
(36) (a) Parr R.G.; Yang W. *Density Functional Theory of Atoms and Molecules*; Oxford University Press: New York, 1989. (b) March, N.H. *Electron Density Theory of Atoms and Molecules*; Academic Press: San Diego, CA, 1992.
(37) Chaban, G.M.; Jung, J.O.; Gerber, R.B. *J. Phys. Chem. A* **2000**, *104,* 2772–2779.
(38) Sobolewski, A.L.; Domcke, W. *J. Phys. Chem. A* **2002**, *106,* 4158–4167.
(39) Del Bene, J.; Perera, S.A.; Bartlett, R.J. *J. Phys. Chem. A* **1999**, *103,* 8121–8124.
(40) Wang, L.; Zhao, J.; Fang, H. *J. Phys. Chem. C* **2008**, *112,* 11779–11785.
(41) Limbach, H.H. In *Hydrogen Transfer Reactions*; Hynes, J.T.; Klinman, J.; Limbach, H.H.; Schowen, R.L., Eds.; Wiley-VCH: Weinheim, Germany, 2007, Vols. 1 and 2, Chapter 6, pp 135–221, and references cited therein.
(42) Janoschek, R. *J. Mol. Struct.* **1994**, *321*, 45–51.
(43) Vendrell, O.; Meyer, H.D. *Phys. Chem. Chem. Phys.* **2008**, *10*, 4692–4703.
(44) Nakahara, M.; Wakai, C. *Chem. Lett.* **1992**, 809–812.
(45) Golubev, N.S. *Khimicheskaya Fizika* **1984**, *3*, 772–774.
(46) Grünberg, B.; Emmler, T.; Gedat, E.; Shenderovich, I.; Findenegg, G.H.; Limbach, H.H.; Buntkowsky, G. *Chem.—Eur. J.* **2004**, *10*, 5689–5696.
(47) Febles, M.; Pérez-Hernández, N.; Pérez, C.; Rodríguez, M.L.; Foces-Foces, C.; Roux, M.V.; Morales, E.Q.; Buntkowsky, G.; Limbach, H.H.; Martín, J.D. *J. Am. Chem. Soc.* **2006**, *128*, 10008–10009.
(48) Bukowski, R.; Szalewicz, K.; Groenenboom, G.C.; van der Avoird, A. *Science* **2007**, *315*, 1249–1252.
(49) Soper, A.K. *Chem. Phys.* **2000**, *258*, 121–137.
(50) Wernet, Ph.; Nordlund, D.; Bergmann, U.; Cavalleri, M.; Odelius, M.; Ogasawara, H.; Näslund, L.Å.; Hirsch, T.K.; Ojamäe, L.; Glatzel, P.; Pettersson, L.G.M.; Nilsson, A. *Science* **2004**, *304*, 995–999.
(51) Smith, J.D.; Cappa, C.D.; Messer, B.M.; Drisdell, W.S.; Cohen, R.C.; Saykally, R.J. *J. Phys. Chem. B* **2006**, *110*, 20038–20045.